International Journal of Solids and Structures 50 (2013) 1332–1341

Contents lists available at SciVerse ScienceDirect

International Journal of Solids and Structures

journal homepage: www.elsevier.com/locate/ijsolstr

A Morphing framework to couple non-local and local anisotropic continua

Yan Azdoud, Fei Han, Gilles Lubineau *

King Abdullah University of Science and Technology (KAUST), Physical Science and Engineering Division, COHMAS Laboratory, Thuwal 23955-6900, Saudi Arabia

ARTICLE INFO

Article history:
Received 11 June 2012
Received in revised form 9 November 2012
Available online 4 February 2013

Keywords:
Non-local elasticity
Coupling
Peridynamics
Long-range forces
Multi-scale
Anisotropy
Morphing

ABSTRACT

In this article, we develop a method to couple anisotropic local continua with anisotropic non-local continua with central long-range forces. First, we describe anisotropic non-local models based on spherical harmonic descriptions. We then derive compatible classic continuum models. Finally, we apply the morphing method to these anisotropic non-local models and present three-dimensional numerical examples to validate the efficiency of the technique.

1. Introduction

Non-local continuum models have the potential to be used in large-scale simulations while taking into account low-scale non-local effects. Promising results have been obtained in fracture analysis of brittle materials (Killic and Madenci, 2009), impact analysis (Demmie and Silling, 2007) and the simulation of progressive damage in composite materials (Askari et al., 2006). Other applications in which non-locality plays an important role, such as nano-reinforced materials or molecular interactions in dissimilar interfaces (Du et al., 2007), are currently under study. Such applications require the development of anisotropic non-local models to capture their strong anisotropic behavior.

We conducted this study in a non-local framework with central long-range forces. In the chosen class of models with central long-range forces, interactions between two material points $\underline{x}$ and $\underline{p}$ are collinear to the bond vector $(\underline{p}-\underline{x})$ and only depend on the displacements of these two points. Such a framework has been extensively described in the literature (Di Paola et al., 2009, 2010; Silling, 2000; Silling and Lehoucq, 2010) with some examples of anisotropic simulation (Askari et al., 2006; Hu et al., 2012), but little work has been done on unified anisotropy. Here, we offer a unified anisotropic framework for non-local models with central long-range forces designed in a simple fashion with the use of spherical harmonics.

As is the case for the isotropic non-local continua, anisotropic non-local continua are expensive to compute. Numerical simulations of non-local continua, while less costly than molecular dynamics, result in complex matrix assemblies. Our previous communication (see Lubineau et al., 2012) addressed this issue through the introduction of a coupling method, which we called the morphing method, with the purpose of using non-local simulation where needed and the classic continuum model (which is less computationally expensive) in the reminder of the structure. Here, we develop the morphing method for a unified anisotropic framework.

This communication is organized as follows. First, we introduce the isotropic non-local framework. In the second part, we develop a framework for orthotropic and transverse isotropic non-local models with central long-range forces and derive compatible local models. Third, we present the morphing method that we adapt here to couple anisotropic non-local models with equivalent local models. Finally, we assess the validity of our approach through numerical examples.

2. An isotropic non-local framework with central long-range forces

In Lubineau et al. (2012), we introduced our morphing method based on an isotropic non-local model with central long-range forces. We briefly review the main features of this model below.

Say that Ω is a continuum where material points interact through long-range forces (see Fig. 1) such that the equilibrium equation at point $\underline{x}$ for a quasi-static problem is:

$$\int_{H_\delta(\underline{x})} \underline{f}(\underline{p}\rightarrow\underline{x})dV_{\underline{p}} + \underline{b} = \underline{0} \quad \forall \underline{x} \in \Omega \tag{1}$$

* Corresponding author. Tel.: +966 28082983.
E-mail address: gilles.lubineau@kaust.edu.sa (G. Lubineau).

0020-7683/$ - see front matter © 2013 Elsevier Ltd. All rights reserved.
http://dx.doi.org/10.1016/j.ijsolstr.2013.01.016

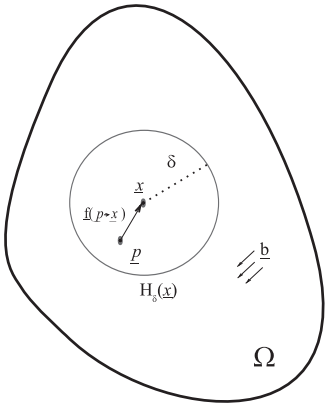

Fig. 1. The non-local continuum $\Omega : H_\delta(\underline{x})$ is the horizon of $\underline{x}$ depending on the characteristic range of long-range forces.

where $\underline{f}(\underline{p} \to \underline{x})$ is the action of point $\underline{p}$ over point $\underline{x}$. δ is the cut-off radius, which limits the long-range interaction of $\underline{x}$ with the material points in its neighborhood, $H_\delta(\underline{x})$ (Fig. 1). $\underline{b}$ are the prescribed external body forces.

To ensure the balance of the linear momentum, an antisymmetric form (with respect to $\underline{x}$ and $\underline{p}$) of the interactions is prescribed (see Silling et al., 2007; Warren et al., 2009). The choice is:

$$\underline{f}(\underline{p} \to \underline{x}) = \hat{\underline{f}}[\underline{x}]\langle \underline{p} - \underline{x}\rangle - \hat{\underline{f}}[\underline{p}]\langle \underline{x} - \underline{p}\rangle \tag{2}$$

where $\hat{\underline{f}}[\underline{x}]\langle \underline{p} - \underline{x}\rangle$ (respectively $\hat{\underline{f}}[\underline{p}]\langle \underline{x} - \underline{p}\rangle$) is the partial interaction due to the action of point $\underline{p}$ over point $\underline{x}$ (respectively of point $\underline{x}$ over point $\underline{p}$). We introduce the bond vector $\underline{\xi} = \underline{p} - \underline{x}$.

If infinitesimal displacements and linear elasticity are assumed, a possible constitutive model is (Silling, 2010; Silling and Lehoucq, 2010):

$$\hat{\underline{f}}[\underline{x}]\langle \underline{p} - \underline{x}\rangle = \frac{c[\underline{x}]}{2}\left\{u_{\underline{\xi}}(\underline{p}) - u_{\underline{\xi}}(\underline{x})\right\}\underline{e}_{\underline{\xi}} \tag{3}$$

where $\underline{e}_{\underline{\xi}} = \underline{\xi}/\|\underline{\xi}\|$ and $u_{\underline{\xi}}(\underline{p})$ is the projection of the displacement at point $\underline{p}$ over the bond (i.e. $u_{\underline{\xi}}(\underline{p}) = \underline{u}(\underline{p}) \cdot \underline{e}_{\underline{\xi}}$). In this approach, the partial bond behaves as a spring with elementary stiffness, $c[\underline{x}]$ (a so-called *micromodulus* in peridynamics). This leads to the set of equations that describes this model over the continuum Ω:

- **Kinematic admissibility and compatibility**

$$\eta_{\underline{\xi}}(\underline{p} - \underline{x}) = u_{\underline{\xi}}(\underline{p}) - u_{\underline{\xi}}(\underline{x}) \quad \forall(\underline{x}, \underline{p}) \in \Omega \tag{4}$$

- **Static admissibility**

$$\int_{H_\delta(\underline{x})} f(\underline{p} \to \underline{x}) dV_{\underline{p}} + \underline{b} = \underline{0} \quad \forall \underline{x} \in \Omega \tag{5}$$

- **Constitutive equation**

$$f(\underline{p} \to \underline{x}) = \frac{c[\underline{x}](\|\underline{\xi}\|) + c[\underline{p}](\|\underline{\xi}\|)}{2}\left\{u_{\underline{\xi}}(\underline{p}) - u_{\underline{\xi}}(\underline{x})\right\}\underline{e}_{\underline{\xi}} \quad \forall \underline{x}, \underline{p} \in \Omega \tag{6}$$

Let us introduce the gradient of the transformation, $\underline{\underline{F}}$, defined as $\underline{\underline{F}} = \frac{\partial \underline{x}}{\partial \underline{X}}$, where $\underline{X}$ is a vector in the reference configuration and $\underline{x}$ its image in the deformed configuration. In case $\underline{\underline{F}}$ is locally uniform, i.e.:

$$\underline{\underline{F}}(\underline{x}') \approx \underline{\underline{F}}(\underline{x}) = \bar{\underline{\underline{F}}} \quad \forall \underline{x}' \in H_\delta(\underline{x}) \tag{7}$$

It has been shown (see Lubineau et al., 2012) that a local model can be defined that is equivalent to a non-local model in an energetic sense. The key-idea is to define the stiffness operator of the local model in such a way that the local and non-local models bear the same strain energy density for any locally uniform strain.

Provided that we consider only small displacements and an homogeneous material ($c[\underline{x}](\|\underline{\xi}\|) = c(\|\underline{\xi}\|)$), this equivalent local model is defined by a 4th-order stiffness operator $\underline{\underline{\underline{\underline{C}}}}$ such that:

$$\underline{\underline{\underline{\underline{C}}}} = \int_{H_\delta(\underline{x})} c^o(\|\underline{\xi}\|) \frac{\underline{\xi} \otimes \underline{\xi} \otimes \underline{\xi} \otimes \underline{\xi}}{2\|\underline{\xi}\|^2} dV_{\underline{p}} \tag{8}$$

From Eq. (8), it is clear that the assumption of central forces results in an additional symmetry of the stiffness tensor, $\underline{\underline{\underline{\underline{C}}}}$ (on top of the classical major and minor symmetries):

$$C_{ijkl} = C_{ilkj} \tag{9}$$

This symmetry implies that some stiffness coefficients are equal. A classic result is that a three-dimensional isotropic continuum can have only one material parameter (the Young's modulus, E), whereas the Poisson's ratio is fixed to $\nu = \frac{1}{4}$. This is also a classic result in atomistic modeling, in which a material represented by a single pair interaction cannot be fully general (Anderson and Demarest, 1971).

Multiple techniques have been developed to tackle this issue and develop totally generic anisotropic models (Gerstle et al., 2007; Silling, 2010; Zhang and Ge, 2005). An overview of those methods is given in Appendix A. Considering that our coupling framework applies to central forces, we develop anisotropic models based only on central forces. In the next section, we present the most general anisotropic description that can be obtained assuming that long-range interactions are central, i.e. parallel to the bond.

3. An anisotropic non-local framework with central long-range forces

3.1. Anisotropy of the micromodulus: notation

In this section, we build an anisotropic model with the restriction of central long-range forces. We start from the isotropic framework presented in Eqs. (1)–(6).

In the isotropic form of Eq. (3), $c[\underline{x}]$ is a local material parameter at point $\underline{x}$ that does not depend on the bond orientation. In order to describe anisotropic behaviors, one possible choice is to express $c[\underline{x}]$ as explicitly depending on the bond's spherical coordinates $(\theta, \phi, \|\underline{\xi}\|$, see Fig. 2) such that:

$$c[\underline{x}] = c[\underline{x}](\theta, \phi, \|\underline{\xi}\|) \tag{10}$$

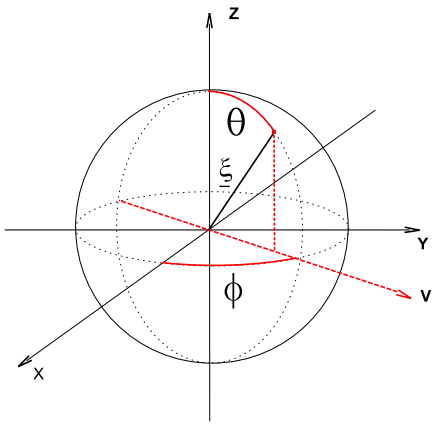

Fig. 2. The bond's spherical coordinates.

Rewriting Eq. (6) leads to:

$$\underline{f}(\underline{p}\to\underline{x}) = \frac{c[\underline{x}](\theta,\phi,\|\underline{\xi}\|) + c[\underline{p}](\pi-\theta,\pi+\phi,\|\underline{\xi}\|)}{2}\left\{u_{\underline{\xi}}(\underline{p}) - u_{\underline{\xi}}(\underline{x})\right\}\underline{e}_{\underline{\xi}} \tag{11}$$

In the case of an homogeneous material (i.e. $c[\underline{x}](\theta,\phi,\|\underline{\xi}\|) = c[\underline{p}](\theta,\phi,\|\underline{\xi}\|) = c(\theta,\phi,\|\underline{\xi}\|)$), we introduce a bond-wise micromodulus $\bar{c}$, so that:

$$\underline{f}(\underline{p}\to\underline{x}) = \bar{c}(\theta,\phi,\|\underline{\xi}\|)\eta_{\underline{\xi}}(\underline{p}-\underline{x}) \tag{12}$$

with

$$\bar{c}(\theta,\phi,\|\underline{\xi}\|) = \frac{c(\theta,\phi,\|\underline{\xi}\|) + c(\pi-\theta,\pi+\phi,\|\underline{\xi}\|)}{2} \tag{13}$$

Provided that $\underline{f}(\underline{p}\to\underline{x})$ derives from a potential $\omega(\eta_{\underline{\xi}}(\underline{p}-\underline{x}),\underline{\xi})$ such that:

$$\underline{f}(\underline{p}\to\underline{x}) = \frac{\partial\omega(\eta_{\underline{\xi}}(\underline{p}-\underline{x}),\underline{\xi})}{\partial\eta_{\underline{\xi}}(\underline{p}-\underline{x})} \tag{14}$$

the strain energy density of the non-local model at a point $\underline{x}$ can be written:

$$W^{nl}(\underline{x}) = \frac{1}{2}\int_{H_\delta(\underline{x})}\omega(\eta_{\underline{\xi}}(\underline{p}-\underline{x}),\underline{\xi})dV_{\underline{p}} \tag{15}$$

$$W^{nl}(\underline{x}) = \frac{1}{4}\int_{H_\delta(\underline{x})}\bar{c}(\theta,\phi,\|\underline{\xi}\|)\left\{u_{\underline{\xi}}(\underline{p}) - u_{\underline{\xi}}(\underline{x})\right\}^2 dV_{\underline{p}} \tag{16}$$

where the factor 1/2 in Eq. (16) relates the bond energy partition between $\underline{x}$ and $\underline{p}$.

We emphasize that $\bar{c}$ has to be centrosymmetric to ensure the conservation of the linear momentum, a property that is met for any choice of c (see the proof in Appendix B). For simplicity and without losing generality, we choose c to be centrosymmetric:

$$c(\theta,\phi,\|\underline{\xi}\|) = c(\pi-\theta,\pi+\phi,\|\underline{\xi}\|) \tag{17}$$

This naturally leads to $\bar{c} = c$. We then drop the bar for convenience.

3.2. Using spherical harmonics to describe the anisotropy

Under the assumption of uniform or smooth strain fields (see Eq. (7)), we can show that an equivalent local model can be derived from the non-local model presented here. Such a model would have a stiffness tensor, $\underline{\underline{\underline{\underline{C}}}}$, defined as follows:

$$\underline{\underline{\underline{\underline{C}}}} = \int_{H_\delta(\underline{x})} c(\theta,\phi,\|\underline{\xi}\|)\frac{\underline{\xi}\otimes\underline{\xi}\otimes\underline{\xi}\otimes\underline{\xi}}{2\|\underline{\xi}\|^2}dV_{\underline{p}} \tag{18}$$

We propose to define c in order to have the most general level of anisotropy under the restriction of central forces. Without any loss of generality we use a real spherical harmonic expansion to describe it:

$$c(\theta,\phi,\|\underline{\xi}\|) = c_{\underline{\xi}}(\|\underline{\xi}\|)\left[a_{00} + \sum_{k=1}^{+\infty}\left[\sum_{m=0}^{k}P_k^m(\cos(\theta))(a_{km}\cos(m\phi) + b_{km}\sin(m\phi))\right]\right] \tag{19}$$

where a_{00}, a_{km} and b_{km} are real parameters, P_k^m are the associated Legendre functions and $c_{\underline{\xi}}$ is a weight function that depends only on $\|\underline{\xi}\|$. This technique is a powerful way to represent general three-dimensional (3D) surfaces (see Thiagarajan et al. (2004) for a description of its application to anisotropy in a virtual bond framework, or Morris et al. (2005) for an application to 3D surface modeling in bioengineering).

3.3. Application to orthotropy and transverse isotropy

3.3.1. An orthotropic model

In the case of an orthotropic material, the model should exhibit three planes of symmetry. Let $(\underline{e}_1,\underline{e}_2,\underline{e}_3)$ be our reference basis. If $(\underline{e}_1,\underline{e}_2,\underline{e}_3)$ is also orthotropic, then c has to satisfy the following relations:

$$\begin{aligned} c(\theta,\phi,\|\underline{\xi}\|) &= c(\pi-\theta,\phi,\|\underline{\xi}\|) = c(\theta,\pi-\phi,\|\underline{\xi}\|) \\ &= c(\theta,\phi+\pi,\|\underline{\xi}\|) \end{aligned} \tag{20}$$

These symmetries lead to the following properties for the equivalent orthotropic stiffness matrix:

$$C_{ijkl} = C_{ijlk} = C_{jikl} = C_{klij} \text{ classical minor and major symmetries} \tag{21}$$

$$C_{ijkl} = C_{ilkj} \text{ central symmetry} \tag{22}$$

$$C_{P(ijkl)} = 0 \text{ if } i\neq(j,k,l) \text{ by antisymmetry of the integrand in Eq. (18)} \tag{23}$$

where $P(\bullet)$ is the permutation operator. A proof of Eq. (23) is given in Appendix C. This leads to the following shape for the stiffness operator using Voigt's notation in the basis $(\underline{e}_1,\underline{e}_2,\underline{e}_3)$:

$$\left[\underline{\underline{\underline{\underline{C}}}}\right]_{(\underline{e}_1,\underline{e}_2,\underline{e}_3)} = \begin{bmatrix} \circledast & \square & \boxdot & 0 & 0 & 0 \\ - & \boxminus & \boxplus & 0 & 0 & 0 \\ - & - & \circledast & 0 & 0 & 0 \\ - & - & - & \square & 0 & 0 \\ - & - & - & - & \boxdot & 0 \\ - & - & - & - & - & \boxplus \end{bmatrix}_{(\underline{e}_1,\underline{e}_2,\underline{e}_3)} \tag{24}$$

As a result, only six independent coefficients are available in an orthotropic model based on central long-range forces, whereas a classical orthotropic material would have nine independent coefficients. We run the model up to the 4th order for Eq. (19) to find those coefficients:

$$c(\theta,\phi,\|\underline{\xi}\|) = c_{\underline{\xi}}(\|\underline{\xi}\|)\left[a_{00} + \sum_{k=1}^{4}\left[\sum_{m=0}^{k}P_k^m(\cos(\theta))(a_{km}\cos(m\phi) + b_{km}\sin(m\phi))\right]\right] \tag{25}$$

Due to the symmetry conditions (Eqs. (17) and (20)) and to the symmetry properties of the associated Legendre functions, it is straightforward to demonstrate that all the coefficients, a_{km} and b_{km}, vanish, except for six of them that do not affect the symmetry properties:

$$[a_{00}, a_{20}, a_{22}, a_{40}, a_{42}, a_{44}] \neq 0 \tag{26}$$

Thus, a 4th-order development of the micromodulus surface provides exactly six material parameters to represent the most general orthotropic materials possible in the framework of central long-range forces. Higher orders of development would not add more generality. The micromodulus surface can be written:

$$\begin{aligned} c(\theta,\phi,\|\underline{\xi}\|) = c_{\underline{\xi}}(\|\underline{\xi}\|)[&a_{00} + a_{20}P_2^0(\cos(\theta)) \\ &+ a_{22}\cos(2\phi)P_2^2(\cos(\theta)) + a_{40}P_4^0(\cos(\theta)) \\ &+ a_{42}\cos(2\phi)P_4^2(\cos(\theta)) + a_{44}\cos(4\phi)P_4^4(\cos(\theta))] \end{aligned} \tag{27}$$

for which the associated Legendre functions are described in Appendix D. Introducing (27) into (18) and performing the necessary integrations provide the relations between the six components of the stiffness tensor and the six parameters of the micromodulus surface:

$$a_{00}=\frac{5(C_{1111}+2C_{1122}+2C_{1133}+C_{2222}+2C_{2233}+C_{3333})}{2\delta^5\pi} \tag{28}$$

$$a_{20}=-\frac{25(C_{1111}+2C_{1122}-C_{1133}+C_{2222}-C_{2233}-2C_{3333})}{4\delta^5\pi} \tag{29}$$

$$a_{22}=\frac{25(C_{1111}+C_{1133}-C_{2222}-C_{2233})}{8\delta^5\pi} \tag{30}$$

$$a_{40}=\frac{45(3C_{1111}+6C_{1122}-24C_{1133}+3C_{2222}-24C_{2233}+8C_{3333})}{16\delta^5\pi} \tag{31}$$

$$a_{42}=-\frac{15(C_{1111}-6C_{1133}-C_{2222}+6C_{2233})}{16\delta^5\pi} \tag{32}$$

$$a_{44}=\frac{15(C_{1111}-6C_{1122}+C_{2222})}{128\delta^5\pi} \tag{33}$$

Eqs. (28)–(33) define the mapping between the local stiffness parameters and the spherical harmonic coefficients for an orthotropic model. Note that those results are valid for $c_\xi(\|\underline{\xi}\|)=1$ if $\|\underline{\xi}\|<\delta$, and $c_\xi(\|\underline{\xi}\|)=0$ otherwise.

3.3.2. A transverse isotropic model

A classical transverse isotropic model would have five independent coefficients. Due to centrosymmetry, our non-local transverse isotropic model has only three coefficients.

Transverse isotropy can be defined by an axisymmetry around the reference direction of the material (here selected as $\underline{e}_3$), which corresponds to the constraints on the micromodulus given in Eq. (34):

$$c(\theta,\phi,\|\underline{\xi}\|)=c(\theta,\|\underline{\xi}\|),\quad c(\theta,\|\underline{\xi}\|)=c(\pi-\theta,\|\underline{\xi}\|) \tag{34}$$

Note that the resulting micromodulus is independent of the angle ϕ. We can then, preserving generality, represent the micromodulus as a development on circular harmonics:

$$c(\theta,\|\underline{\xi}\|)=c_\xi(\|\underline{\xi}\|)\sum_{i=0}^{\infty}a_iP_i^0(\cos\theta) \tag{35}$$

At maximum, a central transverse isotropic model leads to three independent coefficients (Eq. (37)). We limit the circular harmonics development to the minimal expression with three independent coefficients, which is obtained at the 4th order:

$$c(\theta,\|\underline{\xi}\|)=c_\xi(\|\underline{\xi}\|)\left[a_0+a_2P_2^0(\cos\theta)+a_4P_4^0(\cos\theta)\right] \tag{36}$$

$$\left[\underline{\underline{\underline{C}}}\right]_{(\underline{e}_1,\underline{e}_2,\underline{e}_3)}=\begin{bmatrix}\boxplus & \boxdot & \boxslash & 0 & 0 & 0\\ - & \boxplus & \boxslash & 0 & 0 & 0\\ - & - & \circledast & 0 & 0 & 0\\ - & - & - & \boxdot & 0 & 0\\ - & - & - & - & \boxslash & 0\\ - & - & - & - & - & \boxslash\end{bmatrix}_{(\underline{e}_1,\underline{e}_2,\underline{e}_3)} \tag{37}$$

Note that there are four symbols in this matrix: C_{1122} as represented by ⊡ actually depends on the other coefficients.

Using Eq. (36), it leads to

$$a_0=\frac{5(8C_{1111}+12C_{1133}+3C_{3333})}{6\delta^5\pi} \tag{38}$$

$$a_2=-\frac{25(4C_{1111}-3C_{1133}-3C_{3333})}{6\delta^5\pi} \tag{39}$$

$$a_4=\frac{45(C_{1111}-6C_{1133}+C_{3333})}{2\delta^5\pi} \tag{40}$$

The coefficient C_{1122} is defined as:

$$C_{1122}=\frac{1}{3}C_{1111} \tag{41}$$

Note that these results are valid for $c_\xi(\|\underline{\xi}\|)=1$ if $\|\underline{\xi}\|<\delta$ and $c_\xi(\|\underline{\xi}\|)=0$ otherwise.

We have thereby completely defined anisotropic non-local models and their equivalent local models under the assumption of homogeneous transformation. The next step, presented in Section 4, is to generalize the morphing method developed in Lubineau et al. (2012) to perform a natural coupling between the non-local and local models.

4. The morphing technique for anisotropic non-local to local coupling

4.1. The morphing framework

We extend the technique proposed by Lubineau et al. (2012). Specifically, we seek to model a continuum, Ω, where, because of modeling considerations, central long-range forces are required. We use the non-local model only in a sub-domain, Ω_2, which requires a refined description where non-local effects are predominant while, for the remainder of the structure (sub-domain Ω_1), the equivalent local model can be employed. The coupling method is employed in the bridging domain, Ω_m (Fig. 3). The non-local model is defined by the micromodulus $c^o(\theta,\phi,\|\underline{\xi}\|)$ and its equivalent local model by $\underline{\underline{\underline{C}}}^o[\underline{x}]$.

We assume that $\partial\Omega\subset\partial\Omega_1$. The non-local sub-domain, Ω_2, is consequently totally embedded within the local one. Ω_m meets the following requirements:

$$\Omega=\Omega_1\cup\Omega_m\cup\Omega_2;\quad \Omega_1\cap\Omega_m=\emptyset;\quad \Omega_2\cap\Omega_m=\emptyset \tag{42}$$

The coupling is then defined as a simple evolution of the material properties characterizing each model, which leads to the following system of equations:

- **Kinematic admissibility and compatibility**

$$\underline{\underline{\varepsilon}}(\underline{x})=\frac{1}{2}\left(\underline{\nabla}\cdot\underline{u}(x)+{}^t\underline{\nabla}\cdot\underline{u}(x)\right)\quad\forall\underline{x}\quad\in\Omega \tag{43}$$

$$\eta_{\underline{\xi}}(\underline{p}-\underline{x})=u_{\underline{\xi}}(\underline{p})-u_{\underline{\xi}}(\underline{x})\quad\forall(\underline{x},\underline{p})\in\Omega \tag{44}$$

$$\underline{u}=\bar{\underline{u}}\quad\forall\underline{x}\in S_{\bar{\underline{u}}} \tag{45}$$

- **Static admissibility**

$$\underline{div}\,\underline{\underline{\sigma}}+\int_{H_\delta(\underline{x})}\left\{\hat{\underline{f}}[\underline{x}]\langle\underline{p}-\underline{x}\rangle-\hat{\underline{f}}[\underline{p}]\langle\underline{x}-\underline{p}\rangle\right\}dV_{\underline{p}}+\underline{b}=0\ \forall\underline{x}\in\Omega \tag{46}$$

$$\underline{\underline{\sigma}}\cdot\underline{n}=\bar{\underline{T}}\quad\forall\underline{x}\in S_{\bar{\underline{T}}} \tag{47}$$

- **Constitutive equations**

$$\underline{\underline{\sigma}}=\underline{\underline{\underline{C}}}[\underline{x}]:\underline{\underline{\varepsilon}}\quad\forall\underline{x}\in\Omega \tag{48}$$

$$\hat{\underline{f}}[\underline{x}]\langle\underline{p}-\underline{x}\rangle=\frac{c(\theta,\phi,\|\underline{\xi}\|)}{2}\eta_{\underline{\xi}}(\underline{p}-\underline{x})\underline{e}_{\underline{\xi}}\quad\forall\underline{x}\in\Omega \tag{49}$$

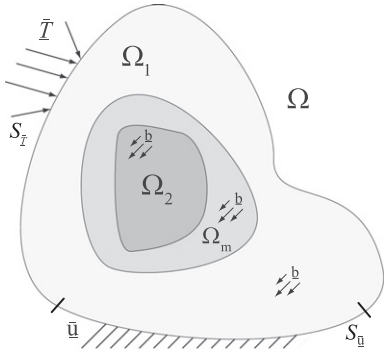

Fig. 3. The domain $\Omega=\Omega_1\cup\Omega_m\cup\Omega_2$.

$\underline{\underline{\underline{\underline{C}}}}[\underline{x}]$ characterizes the stiffness of the local continuum at any point $\underline{x}$. $c(\theta,\phi,\|\underline{\xi}\|)$ is the non-local constitutive parameter at point $\underline{x}$. Using $c^o(\theta,\phi,\|\underline{\xi}\|)$ as references, we define $c(\theta,\phi,\|\underline{\xi}\|)$ by introducing a weighting scalar function, α, such that:

$$c[\underline{x}](\theta,\phi,\|\underline{\xi}\|) = \alpha(\underline{x})c^o(\theta,\phi,\|\underline{\xi}\|) \tag{50}$$

We note that, based on Eq. (46), (Fig. 4):

- a point $\underline{x}$ strictly belongs to the local model (i.e. $\underline{x}\in\Omega_1$) if and only if:

$$\underline{\underline{\underline{\underline{C}}}}[\underline{x}] = \underline{\underline{\underline{\underline{C}}}}^o \quad \text{and} \quad \alpha(\underline{p}) = 0 \quad \forall \underline{p}\in H_\delta(\underline{x}) \tag{51}$$

- a point $\underline{x}$ strictly belongs to the non-local model (i.e. $\underline{x}\in\Omega_2$) if and only if:

$$\underline{\underline{\underline{\underline{C}}}}[\underline{x}] = \underline{\underline{\underline{\underline{0}}}} \quad \text{and} \quad \alpha(\underline{p}) = 1 \quad \forall \underline{p}\in H_\delta(\underline{x}) \tag{52}$$

4.2. Defining the morphing: α and $\underline{\underline{\underline{\underline{C}}}}$

The function α is set to define the interface of the sub-domain Ω_2 as a user parameter. We apply an energy density constraint to define the stiffness tensor $\underline{\underline{\underline{\underline{C}}}}$. At any point $\underline{x}\in\Omega_m$, the strain energy density can be written as:

$$W(\underline{x}) = \frac{1}{2}\underline{\underline{\varepsilon}}(\underline{x}) : \underline{\underline{\underline{\underline{C}}}}(\underline{x}) : \underline{\underline{\varepsilon}}(\underline{x}) + \int_{H_\delta(\underline{x})} c^o(\theta,\phi,\|\underline{\xi}\|)\frac{\alpha(\underline{x})+\alpha(\underline{p})}{2}\frac{\left\{u_{\underline{\xi}}(\underline{p})-u_{\underline{\xi}}(\underline{x})\right\}^2}{4}dV_{\underline{p}} \tag{53}$$

Under a quasi-uniform strain field (Eq. (55)), we can assume that the energy density of the coupling zone is equivalent to the energy density of a fully local model. This is written as:

$$W(\underline{x}) = \frac{1}{2}\underline{\underline{\varepsilon}}(\underline{x}) : \underline{\underline{\underline{\underline{C}}}}^o(\underline{x}) : \underline{\underline{\varepsilon}}(\underline{x}) \tag{54}$$

$$\underline{\underline{F}}(\underline{p}) \approx \underline{\underline{F}}(\underline{x}) = \bar{\underline{\underline{F}}} \quad \forall \underline{p}\in H_\delta(\underline{x}) \tag{55}$$

This naturally leads to a general relation between the stiffness operators:

$$\underline{\underline{\underline{\underline{C}}}}[\underline{x}] = (1-\alpha[\underline{x}])\underline{\underline{\underline{\underline{C}}}}^o + \int_{H_\delta(\underline{x})} c^o(\theta,\phi,\|\underline{\xi}\|)\frac{(\alpha[\underline{x}]-\alpha[\underline{p}])}{2} \times \frac{\underline{\xi}\otimes\underline{\xi}\otimes\underline{\xi}\otimes\underline{\xi}}{2\|\underline{\xi}\|^2}dV_{\underline{p}} \tag{56}$$

Then, provided that the non-local region is fully located by the choice of the morphing function α, the local material parameter $\underline{\underline{\underline{\underline{C}}}}$ can be estimated at every point using Eq. (56). This makes the approach very easy to use as it relies only on the definitions of the changing material parameters across space.

5. Numerical benchmarks and examples

The purpose of this section is to illustrate the accuracy of the coupling method for anisotropic models with three dimensions. We consider two cases. First, we apply the morphing method to an homogeneous orthotropic block under boundary conditions that guarantee uniform strain to evaluate the strain error of the method. As a reference, the same problem is treated as an isotropic model. Second, we study the case of a cracked bulk material under traction and shear using a transverse isotropic model.

In our calculations, we assume the micromodulus $c(\theta,\phi,\|\underline{\xi}\|) = c_\xi(\|\underline{\xi}\|)c_{\theta,\phi}(\theta,\phi)$ to be chosen such that $c_\xi(\|\underline{\xi}\|) = \underline{\xi}^2 e^{-\frac{\|\underline{\xi}\|}{l}}$, where l is an intrinsic length. c_ξ is chosen in such a way as to avoid discontinuities of the bond force (Eq. (46)) at $\underline{\xi}=\underline{0}$ (with the term $\underline{\xi}^2$) and to be small when $\|\underline{\xi}\|=\delta$ (with the exponential term). Numerical implementation of the method is conducted using the Finite Element framework. All elements are eight-node hexahedral elements arranged in a regular grid. The grid size is chosen as 0.02 μm, the intrinsic length is $l = 0.0024$ μm and the horizon δ is 0.06 μm. l can be seen either as a material or phenomenological parameter. Then δ is chosen such that $c_\xi(\|\underline{\xi}\|\geqslant\delta)\simeq 0$ and the ratio of 3 elements per radius δ has been chosen as a compromise between good convergence and calculation time.

Note that the choice of the characteristic length l will not influence elastic characteristics in case of low strain gradients, but rather can be seen as a relevant parameter for other physical effects: at nano-scale, it can approximate Van der Waals forces; in fracture mechanics, it will influence the localization of cracks.

5.1. Example 1: uniform strain of a block

This example aims at presenting an accurate depiction of the coupling effects of an anisotropic non-local bulk in three dimensions. We consider an homogeneous cube subjected to traction and shear conditions. Fig. 5(a) shows the dimensions of this cube. The non-local model is found in the spherical zone Ω_2 colored dark gray in the center of the bulk. The light-gray spherical zone $\Omega_{\overline{m}}$ is the morphing domain over which the weighting function α varies. The rest of this structure is defined with the local continuum model.

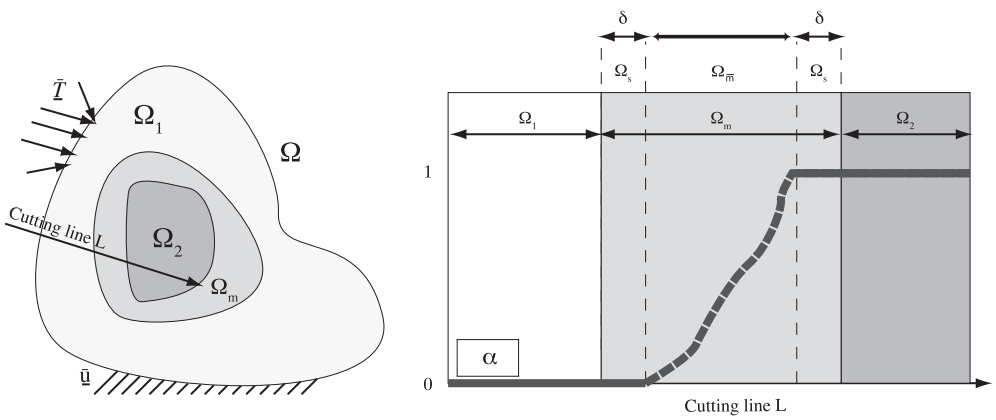

Fig. 4. The general shape of the morphing function α. The solid lines are the initial requirements in Ω_1 and Ω_2 (Eqs. (51) and (52)). The dashed line is a free evolution of α that needs to be defined. Ω_s is a frontier of Ω_m over which α has to be prescribed as either 0 or 1 (see Eqs. (51) and (52)).

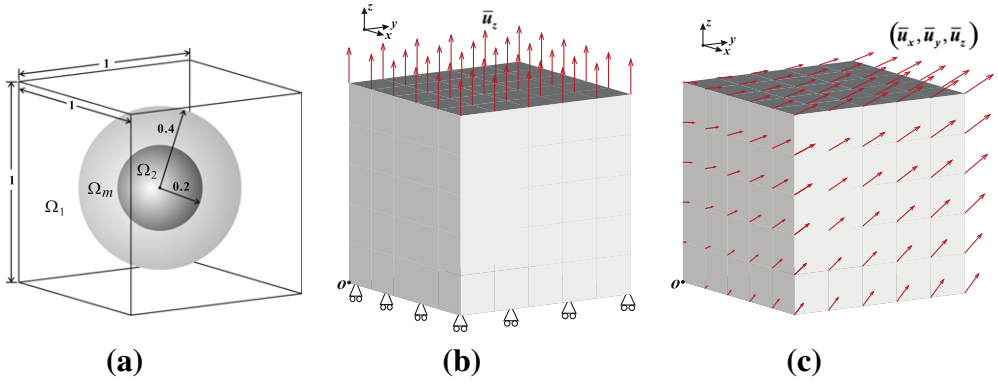

Fig. 5. Dimensions and boundary conditions of a cube (unit of length: μm).

We show the kinematic boundary conditions for the traction case in Fig. 5(b). $\bar{u}_z = 0.5$ μm is the imposed displacement on the top surface of the cube. The displacement is fully prescribed to zero at the origin o (bottom left corner), and the z-component of the displacement is prescribed to zero for all the points over the bottom surface. In a classical local continuum, this would lead to an homogeneous tensile strain field. In Fig. 5(c), the bulk is under pure shear deformation and the kinematic boundary conditions are set by Eq. (57) on all surfaces of the cube:

$$\begin{cases} \bar{u}_x = 0.25y + 0.25z \\ \bar{u}_y = 0.25x + 0.25z \\ \bar{u}_z = 0.25x + 0.25y \end{cases} \tag{57}$$

The equivalent local orthotropic stiffness coefficients for this example are estimated by Eq. (18), and set to $E_x = 60$ GPa, $E_y = 90$ GPa, $E_z = 150$ GPa and $\nu_{xy} = 0.3$, $\nu_{yz} = 0.2$, $\nu_{xz} = 0.1$. The reference isotropic stiffness coefficients are $E = 90$ GPa and $\nu = 0.25$.

Fig. 6 shows the relative error of the strain components, ε_{zz}, obtained for the traction test. The relative error is defined by $\frac{\varepsilon_{zz} - \varepsilon^A_{zz}}{\varepsilon^A_{zz}}$, where ε^A_{zz} is the average value of strain components ε_{zz}. Fig. 6(a) and (c) display the isosurfaces of the relative error in the strain at $+0.05\%$ and -0.05% in a three-dimensional deformed bulk. These isosurfaces limit the regions in which the relative errors in the strain are larger than 0.05%. This reveals that the strain field is quasi-uniform in most of the deformed bulk. We extracted slices perpendicular to the y-axis in which the maximal error is reached ($y = 0.5\,\mu m$), as shown in Fig. 6(b) and (d). Thus, we can clearly see that the spurious effects occur near the upper and lower boundaries of the morphing domain, but, overall, the error in the strain remains at values under 0.3%. In Fig. 6, we compare the result obtained with an isotropic model (a) and (b) with the result obtained with an orthotropic model (c) and (d). The error map is qualitatively the same for both models, demonstrating that the accuracy of the morphing method does not depend of the anisotropic propriety of the model in the case of traction.

The results for the pure shear boundary conditions are shown in Fig. 7. The relative error in ε_{yz} shares similar characteristics with the relative error shown in the traction examples in Fig. 6. Fig. 7(a) and (c) display the isosurfaces set at relative errors of 0.02% and -0.06%, respectively. We show slices on a plane defined by the z-axis and the line $x = y$ on the deformed bulk. This plane has been chosen as it displays the maximal range of the relative error on ε_{yz}. The error range is smaller than in the traction examples in Fig. 6. Again, the anisotropy does not seem to influence the error in the strain induced by the coupling method.

Overall, these two benchmarks demonstrate that the error remains localized to the coupling zone, that the range of error remains small for practical choices of the coupling zone and the coupling function α, and that anisotropy does not qualitatively influence the accuracy of the morphing method.

5.2. Example 2: a cracked block

The benchmark results from previous examples illustrate the quality of the coupling technique. Let us now consider an application. This example is designed to show the performance of the morphing-based coupling technique for representing local phenomena such as those induced by a crack. A cracked bulk is represented in Fig. 8. It is subjected to both traction and shear boundary conditions. The bottom surface of this bulk is completely fixed and

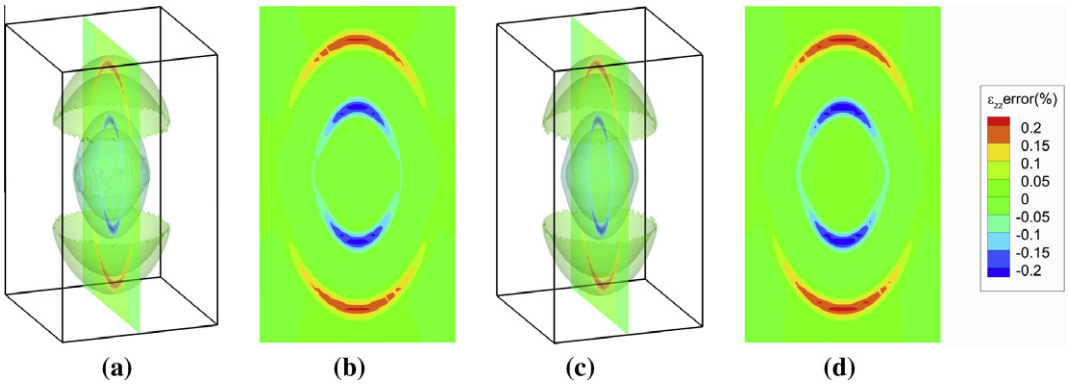

Fig. 6. Isosurfaces (a), (c) and contour slices (b), (d) of the relative error of the strain components ε_{zz} for a 3D bulk under traction with the isotropic stiffness models (a), (b) and with the orthotropic stiffness models (c), (d).

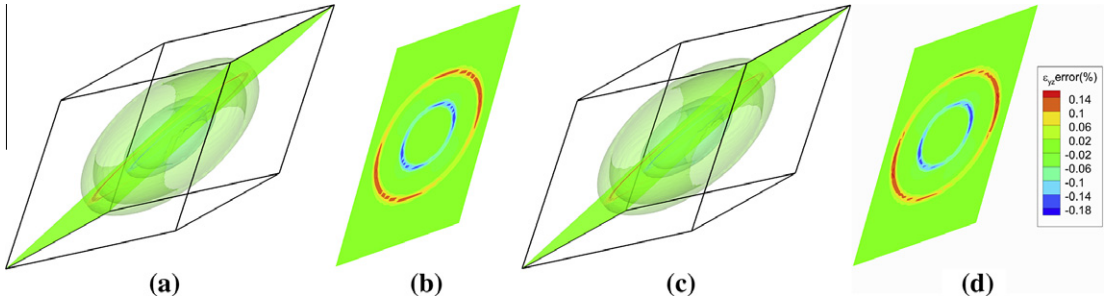

Fig. 7. Isosurfaces (a), (c) and contour slices (b), (d) of the relative error of the strain components ε_{yz} for a 3D bulk under shear with the isotropic stiffness models (a), (b) and with the orthotropic stiffness model (c), (d).

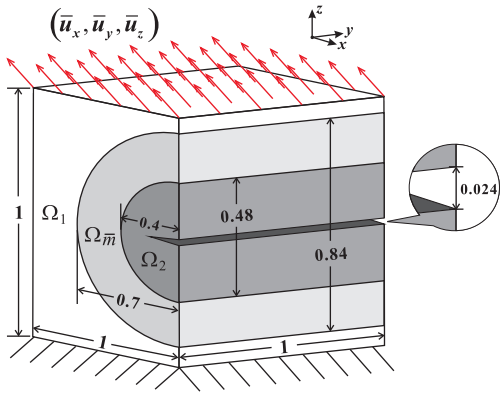

Fig. 8. Dimensions and boundary conditions of a cracked bulk (unit of length: μm).

the values of the boundary displacements on the top surface are given by:

$$\begin{cases} \bar{u}_x = 0\,\mu m \\ \bar{u}_y = 0.5\,\mu m \\ \bar{u}_z = 0.5\,\mu m \end{cases} \tag{58}$$

The non-local continuum model is used in the vicinity of the crack in Ω_2, while classical continuum mechanics is employed in Ω_1. $\Omega_{\overline{m}}$, displayed in light gray (Fig. 8), is the domain where the weighting function α varies. The bulk is modeled as a transverse isotropic material. The stiffness coefficients for the local continuum model are $E_x = E_y = 60$ GPa, $E_z = 150$ GPa and $\nu_{xy} = 0.3$, $\nu_{xz} = \nu_{yz} = 0.1$.

For comparison purposes, the static simulation is run three times, with the classical continuum model, the morphing-based coupling model and the non-local continuum model, respectively. The contour plots of the strain component ε_{xx} are displayed in Fig. 9.

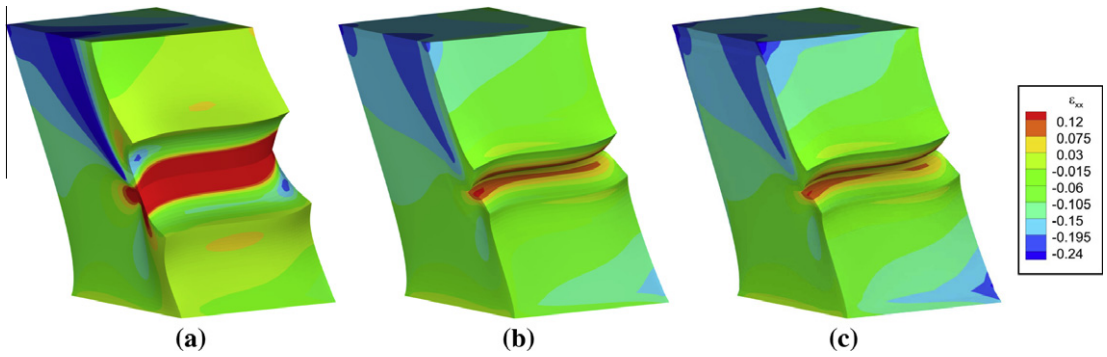

Fig. 9. The strain components ε_{xx} calculated by (a) the classical continuum model, (b) the morphing-based coupling model, and (c) the non-local model.

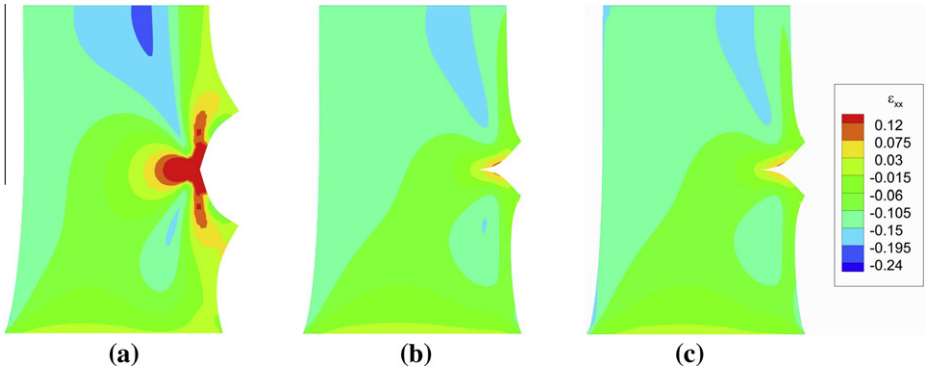

Fig. 10. The contour slices of strain components ε_{xx} calculated by (a) the classical continuum model, (b) the morphing-based coupling model, and (c) the non-local model.

The strain resulting in Fig. 9(a) is obtained by the local continuum model. Its crack shape is different from the others as there is no non-local interaction. Fig. 9(b) shows the solution of the morphing-based coupling model. It has to be compared with results in Fig. 9(c) from the non-local continuum solution.

We plot the slices of the strain component ε_{xx} perpendicular to the y-axis at $y = 0.75\,\mu m$ in Fig. 10 to compare the three models. The results in Fig. 10(b) and (c) indicate similarity, and they differ from the result obtained by the classical continuum model shown in Fig. 10(a). The solutions in Fig. 10(b) and (c) agree, except close to the boundary. This is due to the fact that points near of the surface do not have a complete neighborhood, $H_\delta(\underline{x})$. This mismatch is thus inherent to the differences between local and non-local boundary conditions and is not related to the coupling technique.

This application example shows the adaptability of the morphing method to practical cases, effectively reducing the calculation cost of a non-local simulation while preserving non-locality where it is needed.

6. Conclusion

In this paper, we extended the application field of the morphing method to anisotropic models. The morphing method is a simple and robust method to couple a continuous non-local model with an equivalent local model through a single uniform model defined over the whole structure. We developed the anisotropic model and derived compatible local models in a non-local framework with central long-range forces. A key point of this development is the usage of spherical harmonics to describe the non-local micromoduli. Numerical examples have been provided to demonstrate the efficiency of the method in three dimensions. The morphing method has been shown to be as accurate under anisotropy as under isotropy.

Two main directions are clear for future research. The first is to develop the morphing method for fully generalized anisotropy using considerations presented in Appendix A. The second is to extend the scope of this technique by solving practical mechanical problems using the morphing method.

Appendix A. An overview of anisotropy for long-range-force non-local models

Several methods have emerged to tackle the issue of the central symmetry in large-range interactions based non-local models. It appears that a simple bond consisting of a pair of potentials that depend only on the length of the bond would not be enough to take into account the shear effects. An initial way to circumvent this issue is to take into account multibody interactions: potentials that depend on at least two bonds can introduce a relative rotation. This solution has been chosen, for instance, in the state-based theory (see Silling, 2010). Another way is to further develop the bond-based representation of forces by adding an extra rotational degree of freedom to the material point. This solution is applied in some form to the virtual internal bond method (VIB) (see Zhang and Ge, 2005) and in the work of Gerstle et al. (2007) who uses a Cosserat micro-moduli representation. We describe these methods and evaluate their benefits.

A.1. Multibody interactions

Using multibody interactions to eliminate this symmetry has already been applied in atomistics. Generally, in atomistics, the interaction between particles derives from a potential energy Φ defined as a function of the position of the particles $\underline{x}_i : \Phi(\underline{x}_1, \ldots, \underline{x}_n)$. For instance, a potential energy that depends on the length of pairwise bonds can be written:

$$\Phi = \frac{1}{2}\sum_{i,j} U(\|\underline{x}_i - \underline{x}_j\|) \tag{A.1}$$

where U is the potential of the bond (i,j). It is clear that Eq. (A.1) refers to the stretching energy of the bonds and does not allocate any energy to their relative angular motion. However, if we introduce three-body term potentials, such as the Stillinger–Weber potentials (Stillinger and Weber, 1985), we introduce a relative rotation:

$$\Phi = \frac{1}{2}\sum_{i,j} U(\|\underline{x}_i - \underline{x}_j\|) + \frac{1}{3!}\sum_{i,j,k} V(\|\underline{x}_i - \underline{x}_j\|, \|\underline{x}_j - \underline{x}_k\|, \theta_{ijk}) \tag{A.2}$$

where θ_{ijk} is the angle between the bond (i,j) and the bond (j,k). This process can be extended to more than three particles, but it remains unclear where to truncate the multibody interaction (Volokh and Gao, 2005). A similar point of view is taken for continuum non-local models in the state-based theory by Silling (2010). The model presented by Silling respects the following equations:

- **Kinematic admissibility and compatibility**

$$\underline{\eta}(\underline{x}, \underline{p}) = \underline{u}(\underline{p}) - \underline{u}(\underline{x}) \quad \forall \underline{x}, \underline{p} \in \Omega \tag{A.3}$$

- **Static admissibility**

$$\int_\Omega \underline{T}[\underline{x}]\langle \underline{p} - \underline{x}\rangle - \underline{T}[\underline{p}]\langle \underline{x} - \underline{p}\rangle dV_{\underline{p}} + \underline{b} = 0 \quad \forall \underline{x} \in \Omega \tag{A.4}$$

$$\underline{T}[\underline{x}]\langle \underline{\xi}\rangle = 0 \quad \text{if } \|\underline{\xi}\| \geqslant \delta \quad \forall \underline{x} \in \Omega \tag{A.5}$$

- **Constitutive equation**

$$\underline{T}[\underline{x}]\langle \underline{p} - \underline{x}\rangle = \int_\Omega \underline{\underline{\mathbb{K}}}[\underline{x}]\langle \underline{p} - \underline{x}, \underline{q} - \underline{x}\rangle \underline{\eta}(\underline{x}, \underline{q}) dV_{\underline{q}} \quad \forall \underline{x}, \underline{p} \in \Omega \tag{A.6}$$

$$\underline{\underline{\mathbb{K}}}[\underline{x}]\langle \underline{\xi}, \underline{\zeta}\rangle = 0 \quad \text{if } \|\underline{\xi}\|, \|\underline{\zeta}\| \geqslant \delta \quad \forall \underline{x} \in \Omega \tag{A.7}$$

where $\underline{T}[\underline{x}]\langle \underline{p} - \underline{x}\rangle$ is the *force state* applied at point $\underline{x}$ relative to the bond $\underline{p} - \underline{x}$ and $\underline{\underline{\mathbb{K}}}[\underline{x}]\langle \underline{p} - \underline{x}, \underline{q} - \underline{x}\rangle$ is the *modulus state* that holds the stiffness parameters at point $\underline{x}$ relative to the bonds $\underline{p} - \underline{x}$ and $\underline{q} - \underline{x}$. This system of equations defines the force state $\underline{T}[\underline{x}]\langle \underline{p} - \underline{x}\rangle$ as the association of the direct effects of points $\underline{x}$ and $\underline{p}$ and the indirect effect of their neighborhoods on the bond $\underline{p} - \underline{x}$ (see Fig. 11). In the case of an homogeneous material and under homogeneous deformation, the author gives an equivalent local model in a chosen basis of reference:

$$C_{ijkl} = \int_{H_\delta}\int_{H_\delta} \underline{\underline{K}}_{ik}\langle \underline{\xi}, \underline{\zeta}\rangle \xi_j \zeta_l dV_{\underline{\zeta}} dV_{\underline{\xi}} \tag{A.8}$$

where C_{ijkl} are the equivalent stiffness coefficients and H_δ is a sphere of radius δ in the body Ω. The *modulus state* $\underline{\underline{\mathbb{K}}}$ is a symmetric tensor.

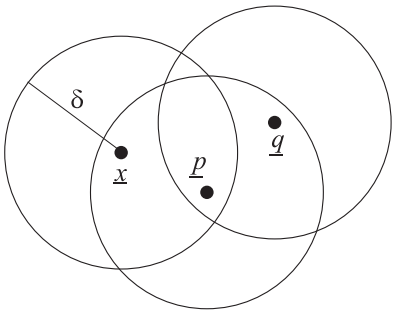

Fig. 11. The point $\underline{q}$ interacts indirectly with $\underline{x}$ because $\underline{p}$ is in the horizon of both $\underline{x}$ and $\underline{q}$.

The symmetries of the stiffness tensor $\underline{\underline{\underline{\underline{C}}}}$ are then the major and minor symmetries. Any classical anisotropy can be reproduced in the non-local framework of the state-based theory.

The evident downside of this method is the high calculation cost that comes from an additional level of integration.

A.2. The Cosserat model

Using an additional set of equations to evaluate the angular behavior of the bond has been applied in the modified virtual internal bond method (Zhang and Ge, 2005), where an additional *R-bond* is introduced. This bond depends on the rotation of a pairwise bond. Another method is introduced in the micropolar peridynamic model presented by Gerstle et al. (2007), based on a Cosserat model. Here, we present the micropolar peridynamic model.

The micropolar peridynamic model relies on a Cosserat continuum extrapolated to a non-local model. The Cosserat model is a contact force model built around the introduction of couples and angles as additional static and, respectively, kinematic variables. Static equilibrium is given by:

$$\sigma_{ji,j} + b_i = 0 \tag{A.9}$$

$$m_{ji,j} + \epsilon_{ijk}\sigma_{jk} + c_i = 0 \tag{A.10}$$

where σ is the Cosserat stress tensor, m is the Cosserat couple, ϵ_{ijk} is the permutation tensor, b_i is the body force and c_i is the body couple force. Cosserat constitutive relations are given by:

$$\sigma_{ij} = D_{ijkl}e_{kl} \tag{A.11}$$

$$m_{ij} = M_{ijkl}\kappa_{kl} \tag{A.12}$$

where $\underline{\underline{\underline{\underline{D}}}}$ and $\underline{\underline{\underline{\underline{M}}}}$ are 4th-order stiffness tensors, $\underline{\underline{e}}$ is the strain operator and $\underline{\underline{\kappa}}$ is the curvature operator. $\underline{\underline{e}}$ and $\underline{\underline{\kappa}}$ are coupled, linked through the relation:

$$\kappa_{ij} = -\epsilon_{ijk}e_{lj,k} \tag{A.13}$$

The author took advantage of this model to create a Cosserat-like peridynamics approach. It increases the size of the system by adding equations on moments in the equilibrium:

$$\int_{H_\delta(\underline{x})} \underline{f}(\underline{p}-\underline{x})dV_{\underline{p}} + \underline{b} = 0 \quad \forall \underline{x} \in \Omega \tag{A.14}$$

$$\int_{H_\delta(\underline{x})} \underline{m}(\underline{p}-\underline{x})dV_{\underline{p}} + \underline{c} = 0 \quad \forall \underline{x} \in \Omega \tag{A.15}$$

where $\underline{f}(\underline{p}-\underline{x})$ (respectively $\underline{m}(\underline{p}-\underline{x})$) is the force (respectively the couple) of $\underline{p}$ over $\underline{x}$.

In three dimensions, a force vector, $\underline{F}_{x,p} = [\underline{f}_x, \underline{m}_x, \underline{f}_p, \underline{m}_p]$, and a kinematic vector, $\underline{U}_{x,p} = [\underline{u}_x, \underline{\theta}_x, \underline{u}_p, \underline{\theta}_p]$, are associated with each bond, (x,p), where $\underline{u}_x$ and $\underline{\theta}_x$ are the displacement and rotation of node x, respectively. The constitutive equation is then given by:

$$\underline{F}_{x,p} = \underline{\underline{K}}_{x,p}\underline{U}_{x,p} \tag{A.16}$$

The stiffness tensor $\underline{\underline{K}}_{x,p}$ is symmetric and depends on parameters of the bond such as its direction, length, effective section and quadratic moment of inertia. Despite the difficulty in associating a physical meaning while choosing these parameters, this model has enough independent variables to completely represent anisotropy in an equivalent Cosserat continuum.

Appendix B. Centrosymmetry of the micromodulus

This section proves that any choice of c leads to a centrosymmetric $\bar{c}$. To satisfy the conservation of linear momentum and under the choice of a centered force, $\bar{c}$ has to be centrosymmetric. Indeed, in a central force representation, the conservation of linear momentum is obtained when:

$$\underline{f}(\underline{p}\to\underline{x}) = -\underline{f}(\underline{x}\to\underline{p}) \tag{B.1}$$

Using Eqs. (11) and (13), it leads to:

$$\bar{c}(\theta,\phi,\|\underline{\xi}\|) = \bar{c}(\pi-\theta,\pi+\phi,\|\underline{\xi}\|) \tag{B.2}$$

Eq. (B.2) being the definition of the centrosymmetry of $\bar{c}$.

By construction, $\bar{c}$ defined as:

$$\bar{c}(\theta,\phi,\|\underline{\xi}\|) = \frac{c(\theta,\phi,\|\underline{\xi}\|) + c(\pi-\theta,\pi+\phi,\|\underline{\xi}\|)}{2} \tag{B.3}$$

is centrosymmetric.

Proof. Let $c(\theta,\phi,\|\underline{\xi}\|)$ be an arbitrary periodical C^1 function. $c(\theta,\phi,\|\underline{\xi}\|)$ can be written as the sum of a centrosymmetric function and a centroantisymmetric function:

$$c(\theta,\phi,\|\underline{\xi}\|) = c_s(\theta,\phi,\|\underline{\xi}\|) + c_a(\theta,\phi,\|\underline{\xi}\|) \tag{B.4}$$

where

$$c_s(\theta,\phi,\|\underline{\xi}\|) = c_s(\pi-\theta,\pi+\phi,\|\underline{\xi}\|) \tag{B.5}$$

and

$$c_a(\theta,\phi,\|\underline{\xi}\|) = -c_a(\pi-\theta,\pi+\phi,\|\underline{\xi}\|) \tag{B.6}$$

Using Eqs. (B.3) and (B.4) yields:

$$\bar{c}(\theta,\phi,\|\underline{\xi}\|) = c_s(\theta,\phi,\|\underline{\xi}\|) \tag{B.7}$$

$\bar{c}(\theta,\phi,\|\underline{\xi}\|)$ is then always centrosymmetric for any choice of $c(\theta,\phi,\|\underline{\xi}\|)$.

As a result, if we choose a centrosymmetric $c(\theta,\phi,\|\underline{\xi}\|)$, we end up with $\bar{c}(\theta,\phi,\|\underline{\xi}\|) = c(\theta,\phi,\|\underline{\xi}\|)$, the choice that we assume for simplification throughout this paper.

Appendix C. Null coefficients in $\underline{\underline{\underline{\underline{C}}}}$

The symmetry property of the integrand of Eq. (18) leads to the null coefficient in the stiffness tensor $\underline{\underline{\underline{\underline{C}}}}$. If we work in a specific basis $(1,2,3)$, Eq. (18) can then be written as:

$$C_{ijkl} = \int_{H_\delta(\underline{x})} c(\theta,\phi,\|\underline{\xi}\|)\frac{\xi_i\xi_j\xi_k\xi_l}{2\|\underline{\xi}\|^2}dV_{\underline{p}} \quad \forall i,j,k,l \in (1,2,3) \tag{C.1}$$

It appears that any permutation of a specific choice of (i,j,k,l) does not change the result of the integrand. Given that there are only three orthogonal directions (namely $(1,2,3)$), we can distinguish three major cases that are not affected by these permutations.

$$i=j=k=l; \quad i=j\neq k=l; \quad i\neq(j,k,l) \tag{C.2}$$

In the third case $(i\neq(j,k,l))$, it is possible to identify that the symmetry property of the integrand will lead to null coefficients of $\underline{\underline{\underline{\underline{C}}}}$. Indeed, the function $c(\theta,\phi,\|\underline{\xi}\|)$ is centrosymmetric and the domain of integration is spherical, centered on $\underline{x}$, which leads to:

- If $j\neq k=l$, $\xi_k\xi_l$ is a centrosymmetric term, ξ_j and ξ_i are antisymmetric and orthogonal, the integrand is antisymmetric: the resulting integral is null.
- If $j=k=l$, $\xi_k\xi_l\xi_j$ and ξ_i are antisymmetric and orthogonal, the integrand is antisymmetric: the resulting integral is also null.

As a result, we obtain Eq. (23):

$$C_{P(ijkl)} = 0 \quad \text{if } i\neq(j,k,l) \quad \forall\ P(i,j,k,l) \text{ permutations of } (i,j,k,l) \tag{C.3}$$

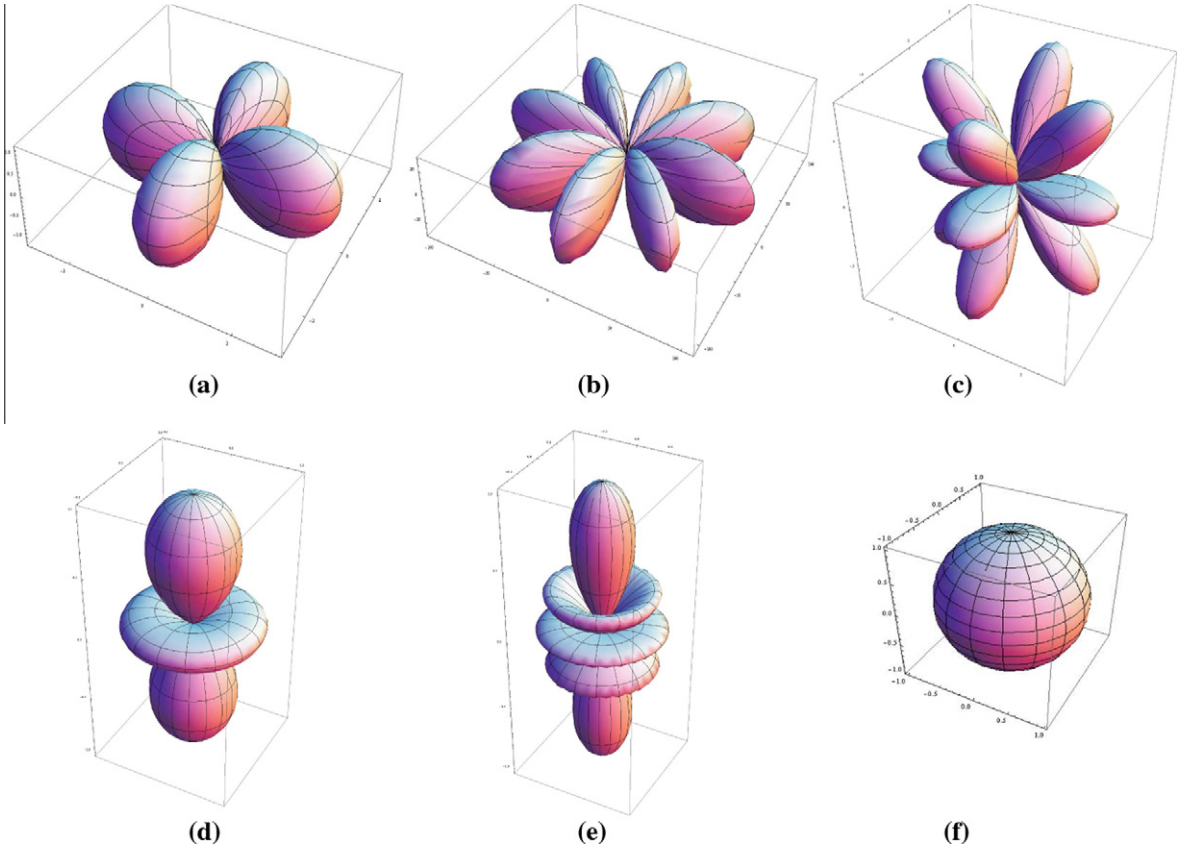

Fig. 12. Spherical harmonics used for the generation of non-local anisotropic models. (a) S_{22} with $a_{22} = 1$ and $b_{22} = 0$, (b) S_{42} with $a_{42} = 1$ and $b_{42} = 0$, (c) S_{44} with $a_{44} = 1$ and $b_{44} = 0$, (d) S_{20} with $a_{20} = 1$, (e) S_{40} with $a_{40} = 1$, (f) S_{00} with $a_{00} = 1$.

Appendix D. Spherical harmonics

Spherical harmonics are built using generalized Legendre polynomials (see Eqs. (D.2)–(D.6)) to create an orthogonal base of function. The base of spherical harmonics S_{ij} (see Fig. 12) is constructed as follows:

$$S_{ij} = P_i^j(cos(\theta))(a_{ij}cos(j\phi) + b_{ij}sin(j\phi)) \quad i,j \in \mathbb{N} \tag{D.1}$$

$$P_2^0(cos(\theta)) = \frac{1}{4}(1 + 3cos(2\theta)) \tag{D.2}$$

$$P_2^2(cos(\theta)) = 3sin(\theta)^2 \tag{D.3}$$

$$P_4^0(cos(\theta)) = \frac{1}{64}(9 + 20cos(2\theta) + 35cos(4\theta)) \tag{D.4}$$

$$P_4^2(cos(\theta)) = \frac{15}{4}(5 + 7cos(2\theta))sin(\theta)^2 \tag{D.5}$$

$$P_4^4(cos(\theta)) = 105sin(\theta)^4 \tag{D.6}$$

References

Anderson, O., Demarest, H., 1971. Elastic constants the central force model for cubic structures: polycrystalline aggregates and instabilities. Journal of Geophysical Research 76, 1349–1369.

Askari, E., Xu, J., Silling, S. 2006. Peridynamic analysis of damage and failure in composites. In: 44th AIAA Aerospace Sciences Meeting and Exhibit, Reno, Nevada.

Demmie, P., Silling, S., 2007. An approach to modeling extreme loading of structures using peridynamics. Journal of Mechanics of Materials and Structures 2, 1921–1945.

Di Paola, M., Failla, G., Zingales, M., 2009. Physically-based approach to the mechanics of strong non-local linear elasticity theory. Journal of Elasticity 97, 103–130.

Di Paola, M., Failla, G., Zingales, M., 2010. The mechanically-based approach to 3D non-local linear elasticity theory: Long-range central interactions. International Journal of Solids and Structures 47, 2347–2358.

Du, J., Bai, J., Cheng, H., 2007. The present status and key problems of carbon nanotube based polymers. Express Polymer Letters 1, 253–273.

Gerstle, W., Sau, N., Aguilera, E. 2007. Micropolar peridynamic constitutive model for concrete. In: SMiRT 19.

Hu, W., Ha, Y., Bobaru, F., 2012. Peridynamic model for dynamic fracture in unidirectional fiber-reinforced composites. Computer Methods in Applied Mechanics and Engineering, 247–261.

Killic, B., Madenci, E., 2009. Prediction of crack paths in a quenched glass plate by using peridynamic theory. International Journal of Fracture 156, 165–177.

Lubineau, G., Azdoud, Y., Han, F., Rey, C., Askari, A., 2012. A morphing strategy to couple non-local to local continuum. Journal of the Mechanics and Physics of Solids 60, 1088–1102.

Morris, R., Najmanovich, R., Karahman, A., Thrnton, J., 2005. Real spherical harmonic expansion coefficients as 3d shape descriptors for protein binding pocket and ligand comparisons. Bioinformatics 21, 2347–2355.

Silling, S., 2000. Reformulation of elasticity theory for discontinuities and long-range forces. Journal of the Mechanics and Physics of Solids 48, 175–209.

Silling, S., 2010. Linearized theory of peridynamic states. Journal of Elasticity 99, 85–111.

Silling, S., Lehoucq, R., 2010. Peridynamic theory of solid mechanics. Advances in Applied Mechanics 44, 73–168.

Silling, S., Epton, M., Weckner, O., Xu, J., Askari, E., 2007. Peridynamic states and constitutive modeling. Journal of Elasticity 88, 151–184.

Stillinger, F., Weber, T., 1985. Computer-simulation of local order in condensed phases of silicon. Physical Review B, 5262–5271.

Thiagarajan, G., Hsia, K., Huang, Y., 2004. Finite element implementation of virtual internal bond model for simulating crack behavior. Engineering Fracture Mechanics, 401–423.

Volokh, K., Gao, H., 2005. On the modified virtual internal bond method. Journal of Applied Mechanics 72, 969–971.

Warren, T., Silling, S., Askari, A., Weckner, O., Epton, M., Xu, J., 2009. A non-ordinary state-based peridynamic method to model solid material deformation and fracture. International Journal of Solids and Structures 46, 1186–1195.

Zhang, Z., Ge, X., 2005. Micromechanical consideration of tensile crack behavior based on virtual internal bond in contrast to cohesive stress. Theoretical and Applied Fracture Mechanics 43, 342–359.